Enhancing K-Band Dual-Input Doherty PA Performance by Bayesian Optimization

Mattia Mengozzi, *Member, IEEE*, Alberto Maria Angelotti, *Member, IEEE*, Gian Piero Gibiino, *Member, IEEE*, Christoph Schulze, *Graduate Student Member, IEEE*, Corrado Florian, *Member, IEEE*, Paolo Colantonio, *Fellow, IEEE*, Olof Bengtsson, *Senior Member, IEEE*, and Alberto Santarelli, *Member, IEEE*

***Abstract*— We present a methodology based on Bayesian optimization (BO) for the performance enhancement of a dual-input Doherty power amplifier (DIDPA) operating at 24 GHz under wideband modulation. First, we implement a dual-input control (DIC) algorithm, which allows for the user-defined arbitrary nonlinear shaping between the two inputs of the DIDPA. Then, an iterative procedure for the performance optimization is configured, where the tuning variables are the bias voltages and the parameters defining the dual-input shaping. Such a procedure jointly targets the improvement of power-added efficiency (PAE) while maintaining linearity by digital predistortion (DPD). To study the feasibility of the method in terms of convergence time and related tradeoffs in performance, the BO is applied in two fashions, namely, one leveraging a quasistatic model (QSM) of the DIDPA and the other directly on modulated signal acquisitions. The experimental results for high peak-to-average power ratio (PAPR) multitone broadband excitations show that the optimized settings can lead to an absolute improvement of several percentage points in PAE compared to the nonoptimized case, while still maintaining a suitable performance in terms of linearity and output power.**

***Index Terms*— Bayesian optimization (BO), digital predistortion (DPD), Doherty power amplifier (PA), power-added efficiency.**

I. Introduction

POWER amplification for high peak-to-average power ratio (PAPR) signals at microwave or millimeter-wave (mm-wave) frequencies, as intended for Frequency Range 2 (FR2) in the fifth generation of telecommunications standards (5G), involves compromising power efficiency for linearity [1]. To mitigate this tradeoff, various power amplifier (PA) topologies have been proposed, such as the Doherty PA (DPA) [2], [3] as well as more advanced architectures incorporating multiple inputs, which are being implemented at both RF [4], [5] and mm-wave frequencies [6], [7], [8]. Among others, the dual-input Doherty PA (DIDPA) [4] features independent RF inputs for the main and auxiliary branches, whereas the load-modulated balanced amplifier (LMBA) [5] makes use of an additional RF input for active load modulation. If suitably adjusted along with the bias voltages, the multiple RF inputs can provide additional degrees of freedom, namely free parameters that can be tuned for PA reconfigurability or to maximize specific performance figures of merit (FoMs).

In this context, previous works have addressed the identification of the optimum shaping between the inputs for DIDPAs [9], [10], [11], outphasing PAs [12], and LMBAs [13]. As a typical approach, an optimal configuration in terms of linearity or power-added efficiency (PAE) is identified heuristically based on the preliminary static characterization of the PA. This step might involve using a look-up table reporting the actual value-based functions for the FoMs or, alternatively, their parameterization. In [13], the performance of an LMBA PA was improved by effectively parameterizing the amplitude and phase relationships of the input split, followed by digital predistortion (DPD) based on neural networks. Indeed, the subsequent application of DPD is usually necessary to achieve satisfactory linearity-efficiency tradeoffs under wideband signal excitation. The work in [9] reports a two-step solution for a DIDPA, where the optimal input for the auxiliary amplifier is derived at first. Then, both inputs are included within the DPD model. In [11], the static splitting functions of a DIDPA are experimentally optimized using an adaptive methodology, followed by DPD applied as a separate step.

Rather than relying on continuous-wave (CW) characterization data, parameter tuning can be made more effective when performed directly on application-like signal regimes, to account for modulated signal statistics and provide weighted FoMs. However, FoMs such as error-vector magnitude (EVM), adjacent-channel power ratio (ACPR), or PAE under wideband modulated conditions can become generally costly to evaluate, since they must be extracted either from lengthy simulations or large measurement datasets. Moreover, parameterizing these metrics to induce a reasonably regular dependency on the tuning variables is not trivial. Yet, iterative optimization algorithms that can automate the tuning of free parameters

Received 6 August 2024; revised 15 October 2024 and 8 November 2024; accepted 9 November 2024. Date of publication 26 November 2024; date of current version 9 June 2025. This work was supported in part by the German Federal Ministry of Education and Research (BMBF) through the Project Forschungsfabrik Mikroelektronik Deutschland under Grant 16FMD02. *(Corresponding author: Gian Piero Gibiino.)*

Mattia Mengozzi, Alberto Maria Angelotti, Gian Piero Gibiino, Corrado Florian, and Alberto Santarelli are with the Department of Electrical, Electronic, and Information Engineering "G. Marconi," University of Bologna, 40136 Bologna, Italy (e-mail: gianpiero.gibiino@unibo.it).

Christoph Schulze and Olof Bengtsson are with the Ferdinand-Braun-Institut (FBH), 12489 Berlin, Germany.

Paolo Colantonio is with the Department of Electronics Engineering, University of Rome Tor Vergata, 00133 Rome, Italy.

Digital Object Identifier 10.1109/TMTT.2024.3498451

are being explored [14], [15]. In [14], the free parameters of an LMBA including input splitting and bias voltages are tuned by heuristic search methods such as simulated annealing. In [15], a derivative-free heuristic algorithm based on simulated annealing and extremum seeking is employed for DIDPAs to maximize a global FoM combining linearity and efficiency. With the exception of [15] (where optimization is repeated based on the DPD performance), it is noteworthy that DPD is usually applied only as a subsequent, separate step after reaching the optimized PA settings. Considering that the output modulated signal after linearization features a different amplitude distribution compared to the case without DPD, and given that the parameter tuning process is normally based on the latter, the obtained linearized performance can substantially deviate from the expected optimum.

In addition, it should be pointed out that characterizing this type of PA involves several practical complexities, including the specific nonlinear operating regimes generated by the multipath/multistage amplification, the presence of multiple bias contacts that must be accessed and adjusted, the use of external predrivers with their own nonidealities, and the need for multiport calibration of broadband measurement paths [16]. Due to these challenges, most cases addressed in the literature focus on sub-6-GHz implementations. Nevertheless, the potential benefits of parameter autotuning and performance improvement would be even more necessary at microwave/mm-wave frequencies. Indeed, compact models' inaccuracies for load-modulated operating conditions are more likely to impact the design phase at these higher frequencies rather than in the well-developed sub-6-GHz range.

This work extends the article in [17] in addressing automated parameter tuning and modulated performance enhancement of an on-wafer microwave monolithic integrated circuit (MMIC) DIDPA operating at 24 GHz, targeting the application to 5G FR2. The device under test (DUT), shown in Fig. 1, is fabricated using the WIN Semiconductors NP15-00 gallium nitride (GaN) on silicon carbide (SiC) technology for mm-wave power applications through 40 GHz. This 0.15-μm-gate-length process is manufactured on 100-mm substrates and uses a source-coupled field plate design to provide the high breakdown voltage required for reliable operation up to 28-V drain–source voltage. High-electron-mobility transistors (HEMTs) with a periphery of 4 $\times$ 50 μm exhibit typical saturated output power of 4.5 W/mm, 12.9 dB linear gain and drain efficiency over 45% at 29 GHz. NP15-00 supports full MMIC designs with transistor layouts for the PA, low-noise amplifier (LNA) and switch functions, two interconnect metal layers, high-reliability metal–insulator–metal (MIM) capacitors, precision tantalum nitride (TaN) resistors, and through-substrate vias for low-inductance ground connections. The main and auxiliary amplifiers include two amplification stages each, with the driver stages realized using 2 $\times$ 75 μm HEMTs, while the final stages are based on 6 $\times$ 75 μm HEMTs. The RF input for the main and auxiliary branches, as well as all gate biases and drain supplies, are all accessible and can be individually controlled.

The measurements are enabled by a state-of-the-art multiport measurement system [18] based on a vector network analyzer (VNA) that is customized in hardware to allow for broadband acquisitions. A dual-input control (DIC) algorithm is here proposed for DIDPA input parameterization, which de-embeds the effects of the external driver amplifiers. By leveraging the multiport calibration of the system, user-defined shaping of the inputs is applied at the DUT on-wafer planes across a 600-MHz bandwidth (BW).

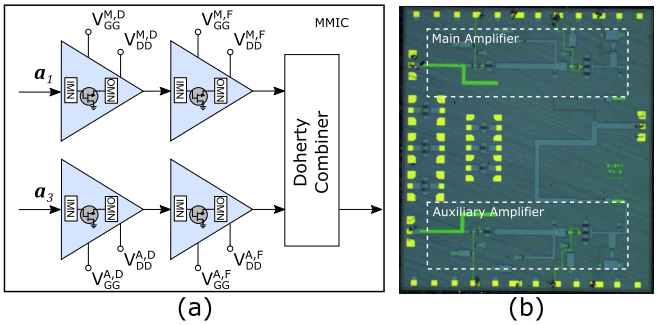

Fig. 1. (a) Block diagram and (b) photograph of the DIDPA in MMIC GaN-on-SiC technology used as the DUT. The processed MMIC also includes additional test devices that are not relevant to this work.

The addressed DIDPA enhancement concerns the improvement of PAE while ensuring a controlled level of linearity. To realize a practical implementation while accounting for input shaping and the many bias voltages, a framework based on the Bayesian optimization (BO) [19] is deployed. Indeed, BO is an excellent candidate for multivariate optimization, as it can theoretically achieve robust heuristics through the exploration of the solutions' space, yet converging to the optimal solution with a relatively small number of evaluations. Bayesian approaches have been previously used in PA design [20], DPD [21], [22], [23] and for behavioral modeling [24]. Regarding the enhancement of multiple-input PAs, preliminary works for DIDPAs showed promising results, for example, BO compared favorably to a coordinate descent approach for the simulation-based evaluation in [25], while in [17], it was successfully applied to the baseline case of a fixed splitting ratio between the two RF inputs. To study the involved optimization tradeoffs, two BO-based approaches are here implemented: the first one is based on multiple evaluations of an approximated quasistatic model (QSM) of the DIDPA, whereas the second one directly relies on wideband modulated measurements (WMMs) without any modeling involved. Unlike the majority of previous implementations, both approaches account for the mutual effect between DPD and PAE maximization across the iterative optimization.

With respect to [17], this work presents a generalized DIC methodology for nonlinear shaping using a new parameterization based on the logistic regression (LR) function, a discussion on optimizing average PAE based on the statistics of the linearized output signal, the implementation of BO for higher dimensionality with up to ten tuning parameters, and a more comprehensive set of experimental test cases comparing linear and nonlinear input shaping. The article is organized as follows. The utilized multiport measurement system is reported in Section II. Section III describes the DIC algorithm, whereas Section IV reports on BO implementation and the different FoMs adopted. The experimental results are

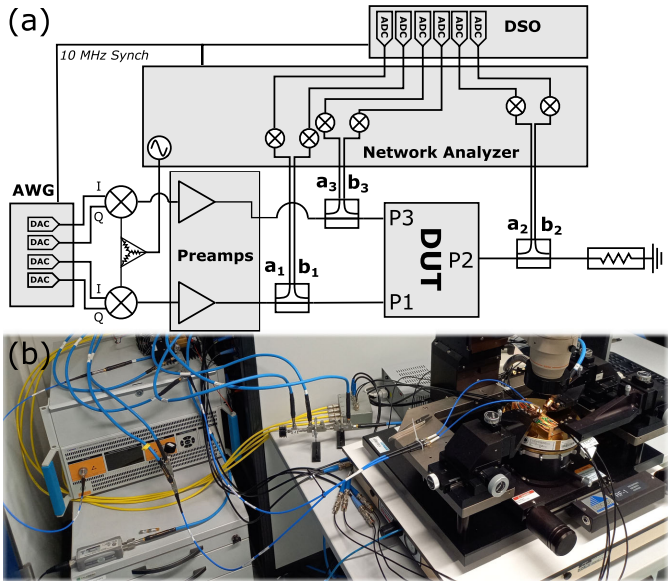

Fig. 2. (a) Block diagram and (b) photograph of the VNA-based three-port measurement system deployed at the FBH institute [18].

summarized in Section V, and conclusions are finally drawn in Section VI.

II. Measurement System

The block diagram and photographs illustrating the on-wafer three-port measurement system, whose detailed implementation can be found in [18], are reported in Fig. 2(a) and (b). External directional couplers and pad attenuators are, respectively, employed to couple the incident/reflected waves and to maximize the dynamic range of the acquisition process. The measurement of the coupled waves is conducted using a specially built four-port Keysight N5247BC PNA-X VNA. In this particular setup, the six IF signals undergo coherent digitization employing a 6-GHz BW digital sampling oscilloscope (DSO Keysight MXR608A). Setup calibration is performed across a 600-MHz BW up to the on-wafer DUT reference planes by employing a short-open-load-thru (SOLT) method including an absolute amplitude step referred to an external power meter.

The excitations at port 1 (P1) and port 3 (P3) are applied through two external IQ mixers driven by a common local oscillator (LO) directly from the internal VNA source. Complex-baseband IQ signals are generated utilizing a Tabor WX2184C arbitrary waveform generator (AWG). Suitable input power levels at the DUT plane should ideally be achieved by using the same bench preamplifiers components for the two inputs, hence minimizing any amplitude and phase mismatches between P1 and P3. However, in this setup, due to limited equipment availability, the P1 branch was preamplified using a cascade of a Miteq AMF-8F-180265 PA and an Erzia ERZ-HPA-2600 PA, while the P3 branch used a Ceyear 3871FP PA. Nevertheless, any asymmetries are here automatically corrected by the DIC procedure treated in Section III-A.

III. Dual-Input Nonlinear Shaping

A. DIC Procedure

As depicted in the block diagram in Fig. 2(a), the modulated signal generated by the AWG inevitably undergoes distortion

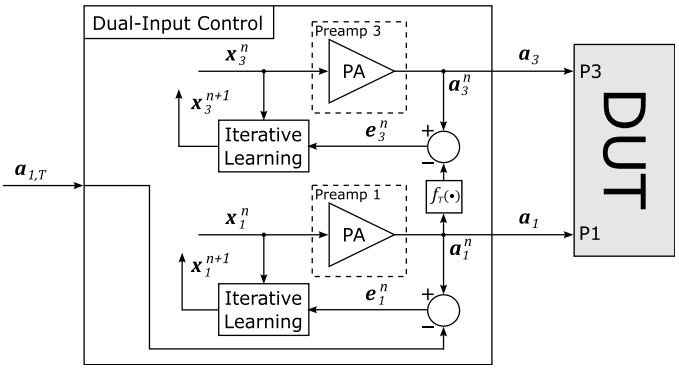

Fig. 3. Block diagram representation of the ILC-based DIC procedure.

in the upconversion and preamplification process. Moreover, these effects may vary from one port to another, resulting in a lack of direct proportionality between user-programmed signals in the AWG (indicated through their time-domain vectors $\mathbf{x}_1$ and $\mathbf{x}_3$ for the two input channels, respectively) and those effectively applied at the DUT on-wafer plane, that is, the complex envelope of the incident waves at ports P1 and P3 (resp. indicated with the time-domain vectors $\mathbf{a}_1$ and $\mathbf{a}_3$ in the following). In general, symmetrical input paths are difficult to achieve, as active devices often exhibit variations even when nominally identical components are used, so corrections are necessary to re-establish precise user control at the DUT on-wafer plane [26].

A constant linear RF input splitting was targeted in the preliminary implementation in [17] by adopting the formulation $\mathbf{a}_3 = \alpha_r e^{j\phi}\mathbf{a}_1$, where α_r and ϕ denote the constant amplitude splitting ratio and the constant relative phase, respectively. Here, we adopt the formulation $\mathbf{a}_3 = f_T(\mathbf{a}_1)$, where $f_T(\cdot)$ is a generic target nonlinear static relationship to be realized through a DIC procedure based on the iterative-learning-control (ILC) algorithm [27]. A representative block diagram for the deployment of the DIC is shown in Fig. 3.

Following the flowchart in Fig. 4, the first step of the DIC is the definition of the P1 target injected wave $\mathbf{a}_{1,T}$ and the target relationship $f_T(\cdot)$. The initial guess $\mathbf{x}_1^0$ for $\mathbf{x}_1$, like in other ILC methods [10], is taken to be proportional to the target value $\mathbf{a}_1^T$. The proportionality constant is empirically determined from an estimate of the equivalent gain for the upconversion and preamplification stages of the first branch. Instead, for the auxiliary branch, the initialization $\mathbf{x}_3^0$ is taken to be proportional to $f_T(\mathbf{x}_1^0)$, where the proportionality factor is determined as in the main branch. The application of these excitation signals will result in initially measured values $\mathbf{a}_1^0$ and $\mathbf{a}_3^0$ for the injected waves that do not generally satisfy $f_T(\cdot)$. Therefore, a setting error is quantified, the next step is calculated, and the procedure is iterated until suitable stop conditions are reached. More in detail, for the nth iteration, the tentative waves $\mathbf{a}_1^n$ and $\mathbf{a}_3^n$ are measured across the entire BW so that the following setting errors e_1^n and e_3^n can be obtained:

$$e_1^n = 20\log_{10}\left(\frac{\left|\left|\mathbf{a}_1^n - \mathbf{a}_{1,T}\right|\right|_2}{\left|\left|\mathbf{a}_{1,T}\right|\right|_2}\right)$$
$$e_3^n = 20\log_{10}\left(\frac{\left|\left|\mathbf{a}_3^n - f_T\left(\mathbf{a}_1^n\right)\right|\right|_2}{\left|\left|f_T\left(\mathbf{a}_1^n\right)\right|\right|_2}\right). \quad (1)$$

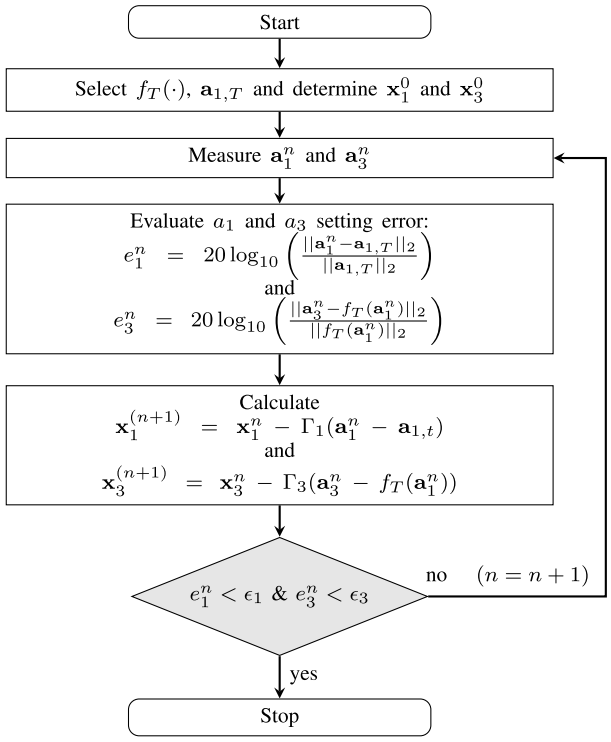

Fig. 4. Simplified flowchart of the ILC-based algorithm for DIC.

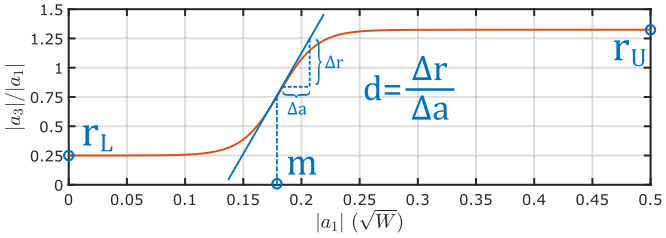

Fig. 5. Parameterization of the nonlinear input shaping of the DIDPA by means of the LR function (i.e., the *sigmoid*).

If these errors are not smaller than the acceptable user-defined values ϵ_1 and ϵ_3, respectively, new tentative AWG digital inputs are calculated by the following ILC-based approach:

$$\begin{aligned}\mathbf{x}_1^{(n+1)} &= \mathbf{x}_1^n - \mathbf{\Gamma}_1\left(\mathbf{a}_1^n - \mathbf{a}_{1,T}\right)\\ \mathbf{x}_3^{(n+1)} &= \mathbf{x}_3^n - \mathbf{\Gamma}_3\left(\mathbf{a}_3^n - f_T\left(\mathbf{a}_1^n\right)\right)\end{aligned} \tag{2}$$

where $\mathbf{\Gamma}_1$ and $\mathbf{\Gamma}_3$ are diagonal matrices realizing separate learning gain settings for each of the inputs. In practice, the overall DIC procedure can be seen as a nested ILC in which the different preamplifiers of the two branches are linearized to generate the target signals $\mathbf{a}_{1,T}$ and $f_T(\mathbf{a}_{1,T})$.

B. Parameterization of the Input Shaping

A suitable parameterization should be found for $f_T(\cdot)$ to allow for the automated tuning of the nonlinear input shaping. In this respect, it can be noted that the DIDPA should take advantage of transitioning from a splitting setting where most input power is injected into the main PA (i.e., at low input powers) to another splitting setting that would involve also the auxiliary branch (i.e., at peak input powers). Hence, one effective solution is adopting the LR function, that is, the *sigmoid* function (see Fig. 5), which is

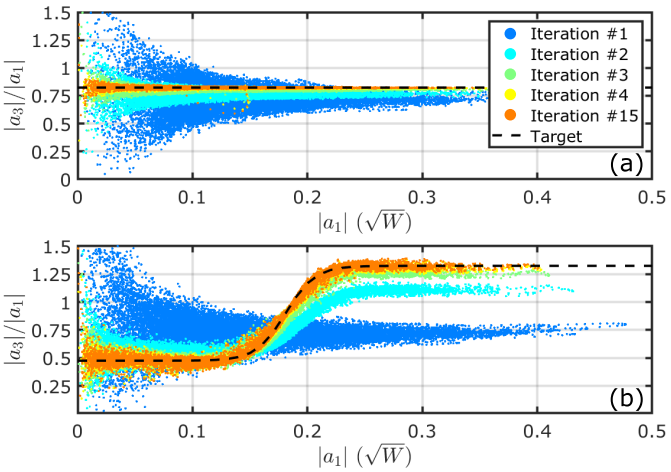

Fig. 6. Iterative behavior of the splitting amplitude when setting. (a) Linear shaping with a splitting ratio $\alpha = 0.6$. (b) Target nonlinear shaping between a_1 and a_3. The injected signal is a 100-MHz BW multitone measured across a BW of 600 MHz.

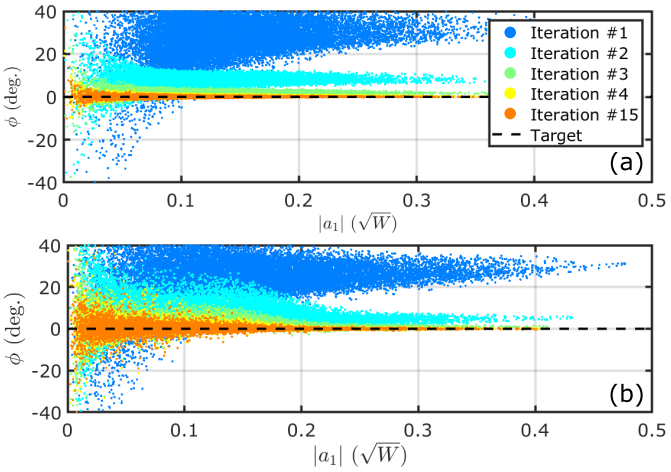

Fig. 7. Iterative behavior of the relative input phase between the two inputs when setting: (a) Linear shaping with a splitting ratio $\alpha = 0.6$. (b) Target nonlinear shaping between a_1 and a_3. The injected signal is a 100-MHz BW multitone measured across a BW of 600 MHz.

particularly appropriate for modeling the transition between two extremal values using a minimal set of parameters. Indeed, while alternative parameterizations, for example, polynomials, could allow for a more elaborate type of nonlinear shaping, they would entail a larger number of parameters, which may lead to overfitting and oscillations. By adopting the notation $\mathbf{a_1} = [a_1(0), a_1(1), \ldots, a_1(i), \ldots, a_1(I-1)]^T$ and $\mathbf{a_3} = [a_3(0), a_3(1), \ldots, a_3(i), \ldots, a_3(I-1)]^T$ for the two input waves, the LR parameterization is analytically defined as

$$a_3(i) = f_{\mathrm{NL}}(a_1(i)) = \left(r_L + \frac{r_U - r_L}{1 + e^{-\frac{4d\left(|a_1(i)|-m\right)}{r_U - r_L}}}\right)e^{-i\phi}a_1(i) \tag{3}$$

where ϕ is the relative phase, m is the turning point of the transition, d corresponds to the slope of f_{NL} at the turning point, whereas r_L and r_U are the lower and upper limits corresponding to the lower (α_L) and upper (α_U) ratio $|a_3(i)|/|a_1(i)|$, respectively:

$$r_L = \sqrt{\frac{1-\alpha_L}{\alpha_L}}; \quad r_U = \sqrt{\frac{1-\alpha_U}{\alpha_U}}. \tag{4}$$

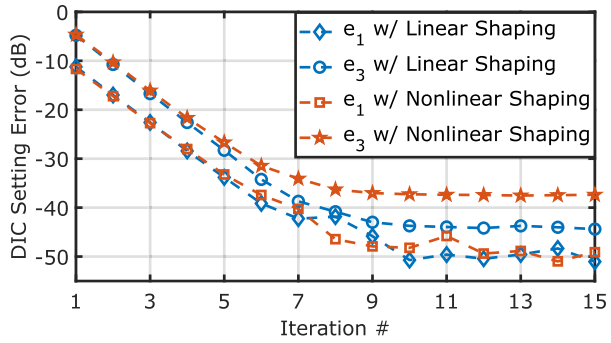

Fig. 8. Setting errors e_1 and e_3 in terms of NMSE between a_1 or a_3 and their respective targets. The different markers indicate whether a linear or nonlinear shaping is set between the two branches.

In the following, the nonlinear shaping parameterization will be comparatively evaluated against the baseline linear shaping which, in this work, is formulated as follows:

$$a_3(i) = f_L(a_1(i)) = \sqrt{\frac{1-\alpha}{\alpha}} e^{-i\phi} a_1(i) \tag{5}$$

where α and ϕ indicate the power splitting ratio and relative phase, respectively. Instead of addressing the ratio $|a_3(i)|\backslash|a_1(i)|$, (5) is based on the power ratio $|a_1(i)|^2\backslash(|a_1(i)|^2 + |a_3(i)|^2)$ to limit α between 0 and 1.

As an example, Fig. 6(a) reports several iterations of the DIC to a target constant $\alpha = 0.6$ in the case of linear splitter emulation, whereas Fig. 6(b) reports the case of a nonlinear LR shaping, while Fig. 7 reports the relative phase ϕ between $\mathbf{a}_1^n$ and $\mathbf{a}_3^n$ for both shapings. Both cases show the possibility to effectively reach the target within a few iterations.

For a better evaluation, the iterative behavior of the corresponding errors e_1 and e_3 reached by the DIC after convergence are reported in Fig. 8. It can be seen that the error e_3 reached for the nonlinear shaping is slightly higher than the corresponding one for the linear splitter. Considering that the target signal features a 100-MHz modulated BW and that the available calibrated BW is limited to 600 MHz, this minor difference can be explained by the larger BW necessary to set the nonlinear shaping between the two inputs.

IV. BO Procedure

A. BO Algorithm

As with any optimization problem, the DIDPA optimization features two principal elements: the definition of the objective function J and the selection of the most suitable algorithm to maximize it. The objective function can correspond to selected FoMs of interest, which depend on the tuning variables $\boldsymbol{\theta} = (\theta_1, \theta_2, \ldots, \theta_R)$, with R being the number of available tuning variables; the optimization problem can then be written as $\max_{\boldsymbol{\theta}} J(\boldsymbol{\theta})$.

The BO algorithm [19] is specifically suitable when the evaluation of $J(\boldsymbol{\theta})$ requires significant time or resources. BO estimates the expected maximum at each iteration based on a surrogate model (SuMo) $\tilde{g}(\boldsymbol{\theta})$ of the objective function, which is extracted from a dataset of past evaluations and iteratively updated. Notably, the SuMO is not a deterministic model, but a stochastic process assigning to each $\boldsymbol{\theta}$ a random variable describing the probability of $J(\boldsymbol{\theta})$ assuming a particular value. A typical SuMo is based on the Gaussian process regression (GPR) [28]. To implement BO, two essential components must be defined.

1) A parametric model for the covariance function of the GPR, resulting in hyperparameters to be updated at each iteration. Common basis functions for this purpose include radial basis functions or squared exponential functions. The *Matern*[1] functions are used here.
2) An acquisition function (AF) to obtain a deterministic value from the GPR-based stochastic prediction. The AF used in this study is the *lower confidence bound*

$$a(\boldsymbol{\theta}) = \mu(\boldsymbol{\theta}) - w\sigma(\boldsymbol{\theta}) \tag{6}$$

where $\mu(\boldsymbol{\theta})$ and $\sigma(\boldsymbol{\theta})$ are the mean and variance of the Gaussian process at the given $\boldsymbol{\theta}$, and w is a scalar parameter tradeoff between exploring unknown points and searching for new optima near the expected ones.

While BO has demonstrated significant success in moderate to low dimensions, extending its application to high-dimensional spaces poses considerable challenges. Indeed, as the dimensionality of the objective function rises, the number of objective function evaluations necessary to span the input space increases exponentially [29]. Given this numerical burden, BO is intended for the one-off tuning of the free parameters in an offline fashion. Once obtained and saved in this preliminary phase, the optimized parameters can then be applied to the corresponding real-time operating regime without incurring any additional numerical burden.

TABLE I
Bias Voltages Used as Tuning Variables

Variable (unit)	Min Value	Max Value	Nominal Value
$V_{GG}^{A,D}$ (V)	-3	-1.5	-2.25
$V_{GG}^{A,F}$ (V)	-3	-1.5	-2
$V_{GG}^{M,D}$ (V)	-3	-1.5	-1.85
$V_{GG}^{M,F}$ (V)	-3	-1.5	-1.83
$V_{DD}^{A,D}$ (V)	5	20	20
$V_{DD}^{A,F}$ (V)	5	20	20
$V_{DD}^{M,D}$ (V)	5	20	20
$V_{DD}^{M,F}$ (V)	5	20	20

B. Tuning Variables

Considering the DUT in Fig. 1, the available quantities that can be controlled by the user are the bias voltages and the parameters of the input signal shaping. Given that each of the two branches of the DIDPA features a two-stage PA, there are four tunable gate voltages (V_{GG}) ranging from the -3 V (pinch-off) to -1.5 V, and four tunable drain voltages (V_{DD}) ranging from 5 to 20 V. As reported in Table I,

[1]Default option in the MATLAB *bayesopt* routine.

TABLE II
TUNING VARIABLES RELATED TO INPUT SIGNAL SHAPING

Variable (unit)	Min Value	Max Value
$^{*}\alpha$ (a.u.)	0	1
$^{*\dagger}\phi$ (deg.)	-180	180
$^{\dagger}\alpha_L$ (a.u.)	0	1
$^{\dagger}\alpha_U$ (a.u.)	0	1
$^{\dagger}m$ ($\sqrt{W}$)	0	0.5
$^{\dagger}d$ ($\frac{\sqrt{\Omega}}{V}$)	0	∞

* Case of linear input shaping.
† Case of nonlinear input shaping.

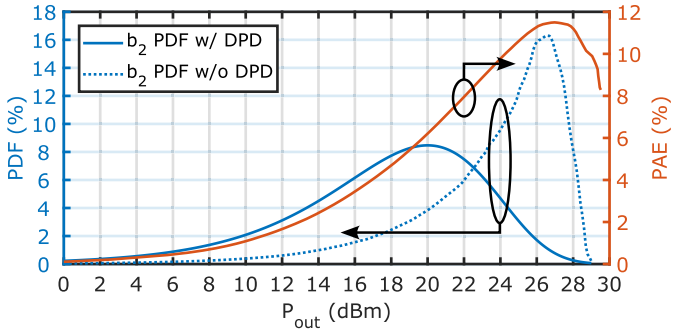

Fig. 9. PAE of the DIDPA under CW conditions (red line) and distribution of the output power levels before DPD (blue dashed line) and after DPD (blue solid line). In this case, the calculated average PAE is 9.1% before DPD and 4.3% after DPD (adopted bias as per nominal values in Table I).

the $(\cdot)^{M,A}$ superscripts, respectively, indicate the main and auxiliary branches, whereas the $(\cdot)^{D,F}$, respectively, indicate the driver and final stages within each branch.

Concerning the input shaping, the DIC procedure will be run at each iteration of the BO to establish a specific relationship between the inputs while maintaining a satisfactorily low error (such as the one reached in Fig. 8). The number of involved parameters depends on the adopted parameterization, as discussed in Section III-B. When the linear splitting in (5) is adopted, the tuning variables are just two, namely α and ϕ. The range for α goes from the situation where all input power is directed to the main branch and no power is directed to the auxiliary PA branch ($\alpha = 1$), to the dual situation where all input power is directed to the auxiliary branch and no power is directed to the main branch ($\alpha = 0$). The relative input phase ϕ ranges from $-180°$ to $180°$.

Beyond the relative phase ϕ, the parameterization for the LR function in (3) features, instead, four tuning parameters (see Fig. 5). The parameters α_L and α_U set the amplitude split at the extremal points of the amplitude range of the input; each of them can range from 0 to 1. If $\alpha_L = \alpha_U = 1$, no power is directed to the auxiliary branch; if $\alpha_L = \alpha_U = 0$, no power is directed to the main branch. The parameter d goes from $d = 0$, corresponding to the case of a constant function, to $d = \infty$, for which the LR function would take the shape of a step function. The turning point can vary between $m = 0$ and $m = 0.5$. All the tuning variables concerning the input shaping are summarized in Table II. The actual set of tuning variables to be considered in the optimization will either involve all the ones listed in Tables I and II, or a suitable subset. In the latter case, the remaining variables are kept to a fixed value.

C. Objective Function

The FoM considered here as the objective for the BO process corresponds to the average PAE of the linearized DIDPA when operated under the target modulated excitation. The PAE is straightforwardly defined as

$$\text{PAE} = \frac{P_{\text{out}} - P_{\text{in}}^{M} - P_{\text{in}}^{A}}{P_{\text{dc}}^{M} + P_{\text{dc}}^{A}} \tag{7}$$

where P_{out} is the output power and P_{in}^{M}, P_{in}^{A}, P_{dc}^{M}, and P_{dc}^{A} are the input and dc absorbed powers of the main and auxiliary branches, respectively.

Devising a way to concurrently impose linearized DIDPA conditions throughout the BO requires analyzing the mutual effect of DPD on PAE. If DPD were applied as a separate final step after running PAE maximization, it would generally impact the operating conditions of the DIDPA, possibly causing a deviation from the achieved optimum. This aspect can be visualized in Fig. 9, where the CW output power vs. PAE characteristic of the DIDPA under test is reported for the nominal values of the free parameters. In nonlinearized conditions, the input signal a_1 follows the statistical distribution dictated by the target modulated signal, whereas the resulting b_2 is distorted, thus featuring a different distribution. After DPD, assuming high-linearity levels are achieved, the output signal b_2 follows the required statistical distribution, whereas a_1 is predistorted. Given that the saturated maximum output power for the PA is fixed, some relevant level of backoff will be caused by DPD, impacting overall performance.

To avoid this detrimental effect, one possible approach would be to setup a multiobjective optimization procedure that jointly accounts for linearity and PAE, as done in [30]. However, this type of approach may present challenges in defining the global optimum that balances the two target metrics, as well as in incorporating additional tuning variables for the DPD, which can, in turn, lead to longer iteration times.

A different approach is instead followed here. The average PAE is evaluated while concurrently imposing linear operation through DPD at each iterative step of the BO. While the optimal predistorted signal for given fixed values of the tuning variables can be obtained through any DPD algorithm available in the literature [31], an ILC-based procedure [27] (see Fig. 10) is used here to directly reconstruct the predistorted waveform without resorting to any parametric DPD implementation. Overall, the following steps are performed at each iteration of the BO.

1) A set of candidate-free parameters for the biases and input splitting of the DIDPA is generated by the BO.
2) The a_1 input is excited with the modulated signal of interest.
3) The a_3 input is iteratively adjusted through the DIC procedure as from Section III-A to satisfy the prescribed input shaping.
4) As the b_2 output is distorted, the a_1 signal is adjusted using ILC to improve the linearity of the DIDPA.

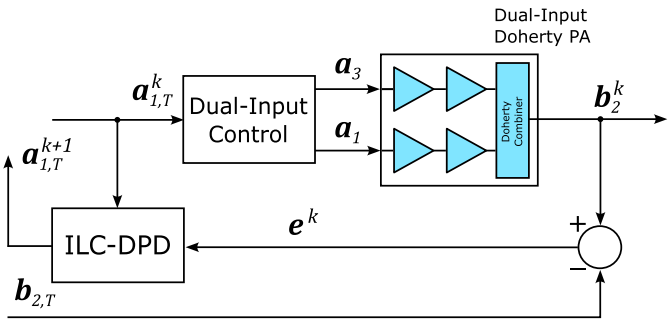

Fig. 10. Block diagram representing the DPD based on the ILC algorithm. Since both the DPD and the DIC in Fig. 3 are based on the ILC approach, their combination effectively realizes a nested ILC procedure (where the DIC is the inner loop and the DPD is the outer loop).

5) Steps 3) and 4) are repeated iteratively until b_2 is linearized (up to the noise floor) and the prescribed a_1–a_3 relationship is jointly enforced.
6) The FoM is evaluated and used by the BO to select the next candidate set of free parameters.

Eventually, the proposed BO implementation is signal-driven, meaning that the resulting optimum depends on the statistics of the input signal. As a consequence, the optimized conditions can be kept fixed for a given signal standard but should, in theory, be re-run if the carrier frequency, BW, or rms power of the input signal is modified. Nevertheless, the optimal settings for a relevant number of signal conditions can be preliminarily characterized offline and then applied during actual PA operation. Concerning DPD, in particular, the use of a nonparametric methodology, as granted by the ILC, allows for the evaluation of the performance ultimately achievable by the DIDPA without constraining the problem to any specific DPD model. Then, in the deployment phase, a DPD model of choice can be selected a posteriori by the user depending on the system requirements (e.g., complexity, real-time constraints, etc.).

It is anyway noteworthy that the overhead in terms of modulated signal acquisitions and postprocessing is generally quite significant, making it worthwhile to investigate more economical ways of running the BO. As introduced in [25], a QSM of the DIDPA can be exploited to provide an estimate of the FoM of interest. Under the hypothesis that the DUT behaves in a purely static way, any given input/output/dc power in (7) can be expressed as a function of the output power as $P(P_{\text{out}})$. To obtain the power value that the QSM would display under the modulated excitation of interest, each $P(P_{\text{out}})$ characteristic has to be statistically averaged by the probability density function (pdf) of the output signal as established by the modulation of interest. This results in the following expression:

$$\hat{P} = \int_0^{+\infty} P(\xi)\text{pdf}_{P_{\text{out}}}(\xi)d\xi \tag{8}$$

where $\hat{P}$ is the estimate of the modulated power to be used in the computations of the FoM, and $\text{pdf}_{P_{\text{out}}}$ is the pdf of the output power in the modulated signal conditions of interest. Clearly, this QSM approach requires knowledge of the quasistatic functions $P(P_{\text{out}})$ for each given set of tuning variables, which can be readily obtained through a quick CW power sweep of the DUT at each iteration of the BO, thus avoiding any lengthy wideband acquisitions. While this process completely discards any existing dynamic memory effects in the DIDPA, it is expected to provide a reasonable approximation of the actual FoM [25].

To mathematically account for the linearization of the DUT while evaluating the average PAE with the QSM approach, it is sufficient to assume that the output power is distributed in the same way as the signal to be amplified, without needing the specification of any DPD. For the wideband signals of interest, which typically display a complex-Gaussian envelope [32], $\text{pdf}_{P_{\text{out}}}$ can be taken to follow an exponential distribution.

In summary, this work considers BO employing two different ways of evaluating the FoM in (7).

1) *QSM:* the FoM is estimated by performing a CW power sweep of the DUT and deriving the required signal performance from (8).
2) *WMM:* the FoM is directly measured from wideband acquisitions of the DUT waves under linearized modulated signal conditions.

V. Measurement Results

The BO implementation follows an offline approach, in which a MATLAB-based routine runs the optimization process and manages the measurement setup. As discussed in Section IV-B, the set of tuning variables for the DIDPA optimization can encompass up to two variables for the linear shaping, and up to five variables for the nonlinear shaping (see Table II). In addition, up to eight bias variables could be considered (see Table I). Hence, accounting for all variables would result in ten variables for the linear input shaping and 13 for the nonlinear one.

However, solving a 13-D BO problem was found to be unfeasible due to the high number of iterations for convergence and the correspondingly excessive tuning time. Indeed, even the time-efficient QSM approach in (8) could generally require the acquisition of several dozen CW power sweeps (one per BO iteration). A strategy was then outlined to perform feasible BOs on a subset of tuning variables, as summarized in Table III along with the adopted naming convention.

The target signal for all cases is a flat-amplitude random-phase multitone with a 100-MHz modulated BW (PAPR = 9.3 dB), matching the circular-complex gaussian pdf typical of 5G signals [32].

A. Linear Input Shaping

Regarding linear input shaping, tests were conducted at increasing dimensionality, starting from the case where only α and ϕ are free parameters, while all bias values are kept fixed at the nominal values as from Table I. A second configuration involved jointly tuning both the input split and the gate bias voltages (six tuning variables in total). Finally, the most demanding test was performed by considering both the input split and all bias variables (ten in total). These configurations were applied to iteratively optimize either the QSM-based PAE

TABLE III
NAMING CONVENTION FOR THE IMPLEMENTED BOS ALONG WITH CONSIDERED FOMS AND TUNING VARIABLES

FoM \ Tuning variables	α, ϕ	α, ϕ, $V_{GG}^{A,D}$, $V_{GG}^{A,F}$, $V_{GG}^{M,D}$, $V_{GG}^{M,F}$	α, ϕ, $V_{GG}^{A,D}$, $V_{GG}^{A,F}$, $V_{GG}^{M,D}$, $V_{GG}^{M,F}$, $V_{DD}^{A,D}$, $V_{DD}^{A,F}$, $V_{DD}^{M,D}$, $V_{DD}^{M,F}$	α_L, α_U, m, d
PAE_{QSM}	QSM-2-L	QSM-6-L	QSM-10-L	QSM-4-NL
PAE_{WMM}	WMM-2-L	WMM-6-L	WMM-10-L	WMM-4-NL

TABLE IV
VALUES OBTAINED FOR THE TUNING VARIABLES AFTER DIDPA OPTIMIZATION*

Test Configuration	α (a. u.)	ϕ (deg)	$V_{GG}^{A,D}$ (V)	$V_{GG}^{A,F}$ (V)	$V_{GG}^{M,D}$ (V)	$V_{GG}^{M,F}$ (V)	$V_{DD}^{A,D}$ (V)	$V_{DD}^{A,F}$ (V)	$V_{DD}^{M,D}$ (V)	$V_{DD}^{M,F}$ (V)
Nominal DPA	0.5	-90°	-2.25	-2	-1.85	-1.83	20	20	20	20
QSM-2-L	**0.45**	**-28°**	-2.25	-2	-1.85	-1.83	20	20	20	20
QSM-6-L	**0.62**	**7°**	**-2.26**	**-2.56**	**-1.76**	**-2.98**	20	20	20	20
QSM-10-L	**0.58**	**-12°**	**-2.08**	**-2.40**	**-1.77**	**-2.56**	**11.6**	**17.3**	**17.1**	**16.0**
WMM-2-L	**0.77**	**-39°**	-2.25	-2	-1.85	-1.83	20	20	20	20
WMM-6-L	**0.74**	**-17°**	**-2.54**	**-2.55**	**-1.83**	**-2.37**	20	20	20	20
WMM-10-L	**0.60**	**-17°**	**-2.31**	**-2.71**	**-1.72**	**-2.72**	**15.8**	**16.8**	**17.1**	**16.7**

*Values resulting from the optimization are highlighted in bold (the others are kept fixed to nominal values).

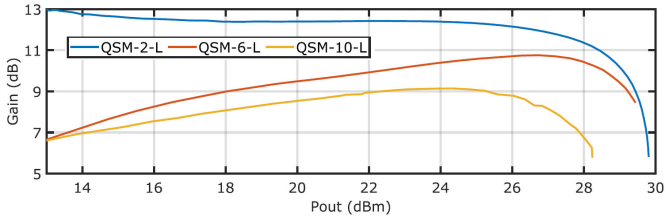

Fig. 11. Static gain characteristic of the optimized DIDPA obtained using the QSM-based approach with different sets of tuning variables as from Table III.

(labeled PAE_{QSM} in Table III) or the actual PAE measured under wideband modulation (labeled PAE_{WMM} in Table III). The values obtained for the free parameters as a result of the BOs are listed in Table IV. For comparison purposes, Table IV also includes the case of the nominal (not optimized) DPA, which features an equal amplitude split and a 90° phase shift between the two inputs.

Fig. 11 presents the quasistatic gain and PAE characteristics obtained from running the QSM-based approach. These display an uncommon shape, as they result from targeting the PAE with the weighting function in (8) as based on the pdf of the modulated signal. Hence, they are unfit for CW operation. These plots are nevertheless useful in illustrating that when the bias voltages are included among the free parameters, they have a substantial impact on the characteristics. Indeed, when the drain voltages are kept fixed at the nominal 20 V, the gate voltages of the final stages are pushed toward lower values (see Table IV), thus moving toward more power-efficient and nonlinear regimes. When also the drain voltages are left free to change, they get reduced by up to 4 V, and the input split and gate bias values are adjusted accordingly. The PAE characteristics are correspondingly pushed toward higher values, whereas gain is progressively reduced.

The worsening of the linearity seen in Fig. 11 is, anyway, only apparent. As discussed in Section IV-C, the QSM-based methodology accounts for a theoretical inversion of the quasistatic input–output characteristic by considering the distribution of the linearized output signal. In other words, it inherently assumes that the final configuration will exploit DPD. The actual linearity performance must then be evaluated after DPD for the actual case of wideband modulated excitation.

TABLE V
DIDPA PERFORMANCE AS EXPERIMENTALLY TESTED BY WMMS (INCLUDING DPD)

Test Configuration	PAE (%)	P_{out}^{RMS} (dBm)	P_{in}^{RMS} (dBm)	EVM (dB)	ACPR (dB)
Nominal DPA	4.3	18.4	8.3	-39.2	-44.1
QSM-2-L	6.8	20.0	7.6	-49.7	-52.6
QSM-6-L	9.9	19.9	10.4	-37.7	-40.0
QSM-10-L	12.9	20.0	11.2	-48.8	-51.1
WMM-2-L	6.8	19.9	7.9	-49.0	-55.4
WMM-6-L	9.2	20.5	10.7	-44.7	-49.2
WMM-10-L	12.7	20.0	10.9	-49.7	-52.6
QSM-4-NL	13.5	19.7	10.4	-48.5	-54.5
WMM-4-NL	13.2	19.9	10.8	-46.2	-48.9

In this respect, Fig. 12 reports the measured validations for the DIDPA tuned as per the QSM-based approaches, showing that DPD can recover linearity. This is quantitatively proven in terms of EVM and ACPR, respectively, resulting in the approximate range of -45 to -50 dB for both the QSM-2-L and QSM-10-L cases (see Table V). The optimum found for the QSM-6-L results in a slightly higher peak RF output power, and a correspondingly slightly lower linearity metrics. Table V also reports the values of the average PAE, showing a progressive increase from 6.8% to 12.9% as the bias voltages are included, yet maintaining similar values in terms of RF output power and linearity. The BO results for the WMM configurations are mostly aligned to QSM in terms of PAE improvement and linearity performance (see Fig. 13 and Table V). Some slight deviations can be seen for the WMM-6-L case, which shows some improvement in linearity, effectively aligning with the two other test cases, while displaying the highest peak RF power of all tested cases.

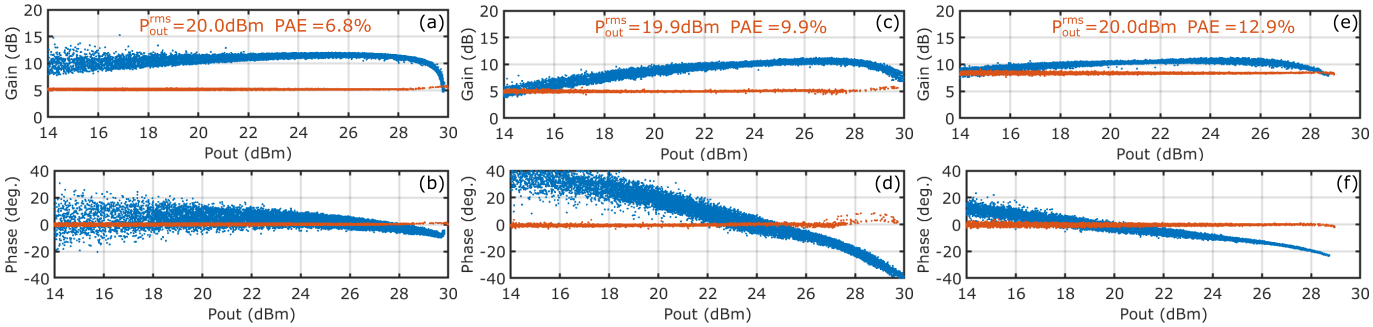

Fig. 12. DIDPA gain and phase characteristics w/ and w/o DPD (red and blue lines, respectively) for the following optimization configurations as from Table III. (a) and (b) QSM-2-L. (c) and (d) QSM-6-L. (e) and (f) QSM-10-L.

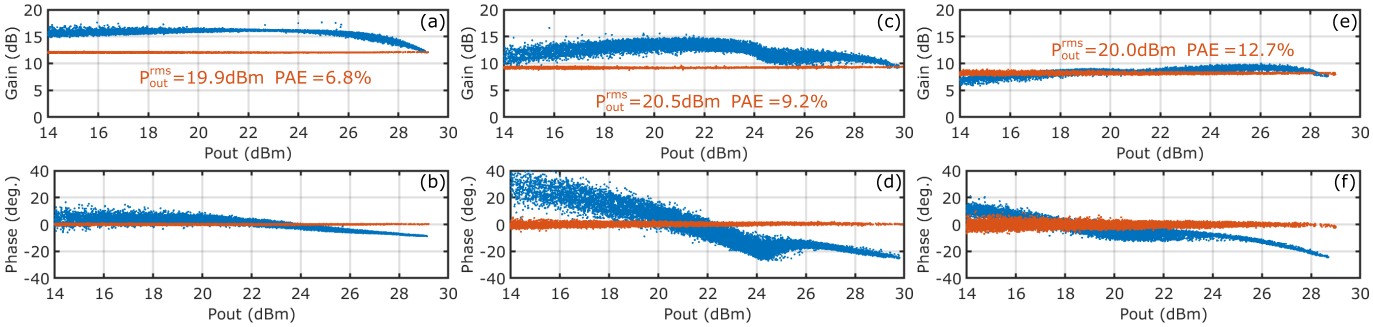

Fig. 13. DIDPA gain and phase characteristics w/ and w/o DPD (red and blue lines, respectively) for the following optimization configurations as from Table III. (a) and (b) WMM-2-L. (c) and (d) WMM-6-L. (e) and (f) WMM-10-L.

TABLE VI

VALUES OBTAINED FOR THE TUNING VARIABLES OF THE LR FUNCTION DEFINING THE NONLINEAR INPUT SHAPING

	α_L (a.u.)	α_U (a.u.)	m ($\sqrt{W}$)	d ($\frac{\sqrt{\Omega}}{V}$)
QSM-4-NL	0.81	0.36	0.18	20
WMM-4-NL	0.96	0.30	0.14	20

These results seem to demonstrate that, for this DUT, the time-efficient QSM can lead to a good prediction of the DIDPA behavior, so that the QSM-based BO is effective in autotuning the DIDPA. Nevertheless, the resulting values for the tuning variables are not the same between the QSM and WMM cases, with some differences in terms of the input split. This suggests a different optimization path for the two configurations and that similar global DIDPA performance can be reached by different combinations of the tuning variables. This, in turn, highlights the presence of multiple suitable solutions as a consequence of the many degrees of freedom and the irregularity of the target FOM.

In this respect, it is worth analyzing the iterative behavior shown in Fig. 14, where the reported PAE values correspond to the values of the objective function at each iteration of the BO. Each iteration corresponds to a CW sweep for the QSM cases or to a wideband modulated acquisition (beyond those for DIC and DPD) for the WMM cases. As could be expected, the convergence is proportionally slower as the number of tuning variables is increased.

B. Nonlinear Input Shaping

To implement a feasible BO of the nonlinear input shaping, we leverage the results obtained in the case of linear shaping.

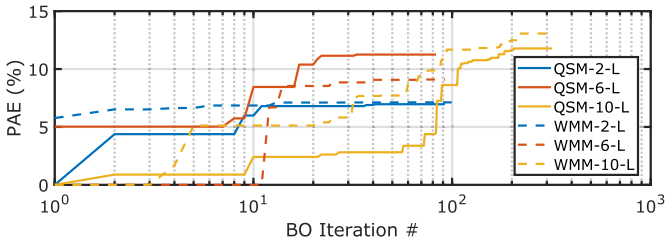

Fig. 14. Trajectory of the average PAE (set as the objective function) across the iterations of the BO for the QSM and WMM cases when using linear input shaping (see Table III). For the QSM cases, the PAE is calculated at every iteration by the QSM; as such, the calculated PAE after convergence is slightly different from that finally measured under modulation. For WMM cases, the PAE is directly acquired from modulated measurements at each iteration.

In fact, we retain the optimal bias and relative phase values, respectively, found for the QSM-10-L and WMM-10-L tests, so to conduct two new corresponding BOs (referred to as QSM-4-NL and WMM-4-NL, respectively) where only the four free parameters of the LR function are considered. This choice allows us to focus on the additional performance improvement due to nonlinear shaping.

The obtained results are reported in the two last lines of Table V, showing a further improvement in terms of average PAE for similar values of the other metrics. Moreover, the DPD still allows for the recovery of high levels of linearity for both cases, as demonstrated by the low levels of EVM and ACPR. These results are also displayed in terms of dynamic gain and phase responses in Figs. 15 and 16, and the linearized spectra in Fig. 17(a) and (b).

The resulting optimal input shaping and related free parameters of the LR function are shown in Fig. 18 and Table VI.

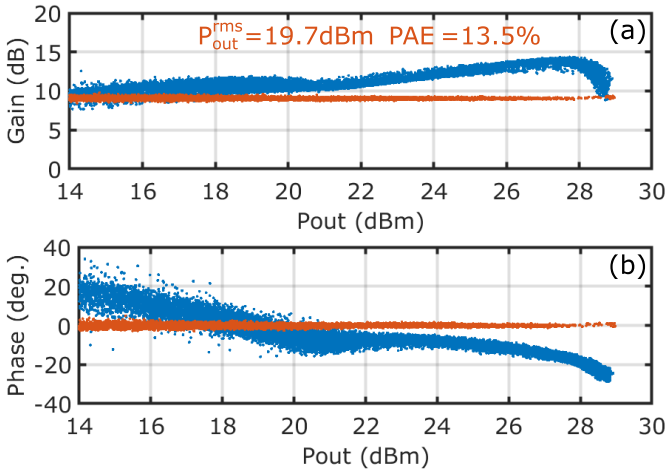

Fig. 15. (a) Gain and (b) phase characteristics w/ and w/o DPD (red and blue lines, respectively) for the QSM-4-NL case (see Table III), which involves nonlinear input shaping.

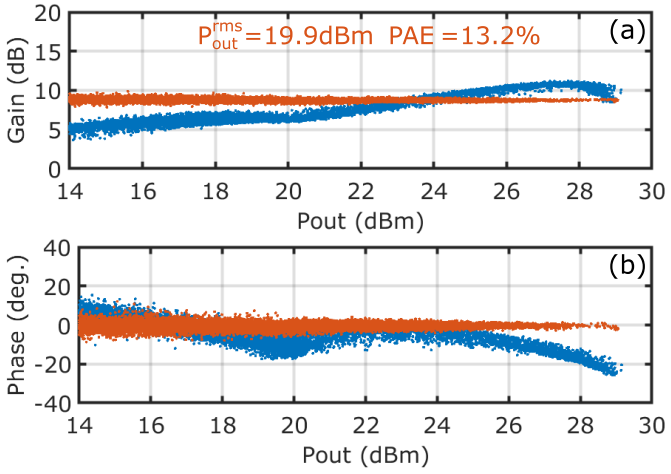

Fig. 16. (a) Gain and (b) phase characteristics w/ and w/o DPD (red and blue lines, respectively) for the WMM-4-NL case (see Table III) which involves nonlinear input shaping.

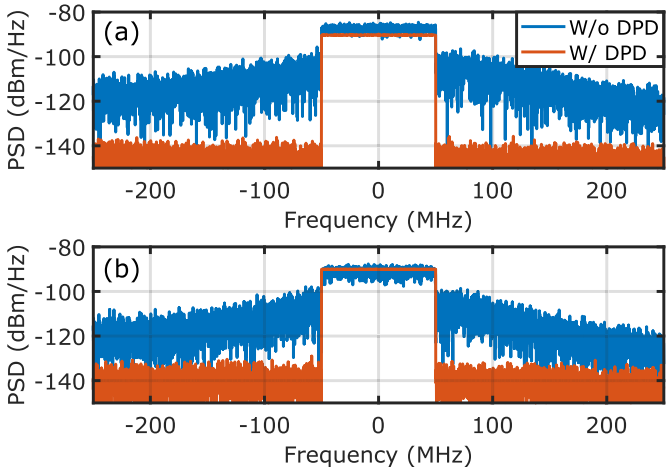

Fig. 17. Output spectra before and after DPD for the configurations (a) QSM-4-NL and (b) WMM-4-NL (see Table III).

The input shaping gets adapted to the two different bias configurations, hence resulting in two different control functions.

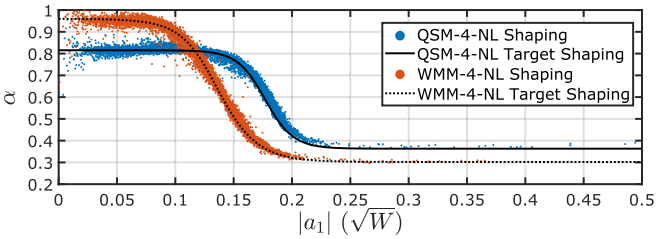

Fig. 18. Nonlinear input shaping realized by the DIC resulting from the 4-QSM-NL and 4-WMM-NL configurations (see Table III) based on the parameterization of the LR function (see Table VI).

For both cases, the parameter d effectively imposes two different levels for the shaping, thus defining the different dynamic feeding of the main and auxiliary branches along the instantaneous power. At the same time, provided that d falls into a suitable and relatively wide range ($1 < d < 100$), the performance results are found to be barely dependent on the actual slope imposed by d.

Notably, Fig. 18 reports both the targeted shaping (dashed and solid black lines) as well as the measured shaping under modulated excitation, further demonstrating the effectiveness of the DIC algorithm in setting the wanted shaping in this specific optimal wideband solution.

VI. Conclusion

This article illustrated an input-control methodology aimed at maximizing the PAE of a K-band DIDPA while maintaining high linearity and output power across a wide modulated BW. The outlined procedure allows to impose of an arbitrary nonlinear relationship between the wideband inputs at the on-wafer MMIC plane. A suitable parametric description of such a relationship enables the dual-input shaping of the DIDPA to be automatically tuned together with the bias values through multidimensional optimization routines. The adopted optimization, based on a Bayesian approach, jointly accounts for linearization and PAE maximization, avoiding any suboptimal deviations that could have occurred if the DPD was applied only at the end of the procedure, as a separate step.

When comparing the achieved results to the case where only the input amplitude ratio and phase shift were optimized, an absolute improvement of several percentage points in PAE was obtained, with similar levels of output power and both EVM and ACPR maintained well below -45 dB for a 9-dB PAPR, 100-MHz modulated input signal. This resulted in an overall enhancement, ultimately achieving performance comparable to those reported in the K-band for PAs in GaN technology operating under similar conditions [2], [3].

The presented validation campaign also included an implementation leveraging a QSM of the DIDPA, which is aimed at minimizing the overall optimization time. This reported only minor differences in the obtained DIDPA performance with respect to the case where optimization directly exploited modulated measurements.

Given the ever-increasing need for flexible PA operation, reconfigurable PAs with a high level of tunability are currently being investigated [33]. As a result, this kind of optimization methodology will be a critical aspect of future PA modules.

ACKNOWLEDGMENT

The authors would like to thank the Microwave Engineering Center for Space Applications (MECSA) and WIN Semiconductors for providing access to the NP15-00 150-nm GaN-on-SiC process.

REFERENCES

[1] C. Fager, T. Eriksson, F. Barradas, K. Hausmair, T. Cunha, and J. C. Pedro, "Linearity and efficiency in 5G transmitters: New techniques for analyzing efficiency, linearity, and linearization in a 5G active antenna transmitter context," *IEEE Microw. Mag.*, vol. 20, no. 5, pp. 35–49, May 2019.

[2] K. Nakatani, Y. Yamaguchi, Y. Komatsuzaki, S. Sakata, S. Shinjo, and K. Yamanaka, "A Ka-band high efficiency Doherty power amplifier MMIC using GaN-HEMT for 5G application," in *IEEE MTT-S Int. Microw. Symp. Dig.*, Aug. 2018, pp. 1–3.

[3] R.-J. Liu et al., "A 24–28-GHz GaN MMIC synchronous Doherty power amplifier with enhanced load modulation for 5G mm-Wave applications," *IEEE Trans. Microw. Theory Techn.*, vol. 70, no. 8, pp. 3910–3922, Aug. 2022.

[4] R. Darraji, F. M. Ghannouchi, and O. Hammi, "A dual-input digitally driven Doherty amplifier architecture for performance enhancement of Doherty transmitters," *IEEE Trans. Microw. Theory Techn.*, vol. 59, no. 5, pp. 1284–1293, May 2011.

[5] R. Quaglia and S. Cripps, "A load modulated balanced amplifier for telecom applications," *IEEE Trans. Microw. Theory Techn.*, vol. 66, no. 3, pp. 1328–1338, Mar. 2018.

[6] B. Rabet and J. Buckwalter, "A high-efficiency 28 GHz outphasing PA with 23 dBm output power using a triaxial balun combiner," in *IEEE Int. Solid-State Circuits Conf. (ISSCC) Dig. Tech. Papers*, Feb. 2018, pp. 174–176.

[7] N. Rostomyan, M. Özen, and P. Asbeck, "A ka-band asymmetric dual input CMOS SOI Doherty power amplifier with 25 dBm output power and high back-off efficiency," in *Proc. IEEE Topical Conf. RF/Microwave Power Model. for Radio Wireless Appl. (PAWR)*, Jan. 2019, pp. 1–4.

[8] D. N. Martin, P. Enrico de Falco, M. Roberg, G. Lasser, and T. W. Barton, "An 18–38-GHz K-/Ka-band reconfigurable Chireix outphasing GaAs MMIC power amplifier," *IEEE Trans. Microw. Theory Techn.*, vol. 68, no. 7, pp. 3028–3038, Jul. 2020.

[9] H. Cao, H. M. Nemati, A. Soltani Tehrani, T. Eriksson, and C. Fager, "Digital predistortion for high efficiency power amplifier architectures using a dual-input modeling approach," *IEEE Trans. Microw. Theory Techn.*, vol. 60, no. 2, pp. 361–369, Feb. 2012.

[10] J. C. Cahuana, P. Landin, D. Gustafsson, C. Fager, and T. Eriksson, "Linearization of dual-input Doherty power amplifiers," in *Proc. Int. Workshop Integr. Nonlinear Microw. Millimetre-wave Circuits (INMMiC)*, Apr. 2014, pp. 1–3.

[11] J. Peng, S. He, W. Shi, T. Yao, J. Wu, and J. Wang, "Adaptive signal separation for dual-input Doherty power amplifier," *IEEE Trans. Microw. Theory Techn.*, vol. 68, no. 1, pp. 121–131, Jan. 2020.

[12] W. Li et al., "Performance modeling and shaping function extraction for dual-input load modulated power amplifiers," in *IEEE MTT-S Int. Microw. Symp. Dig.*, Jun. 2023, pp. 203–206.

[13] E. Guillena, W. Li, G. Montoro, R. Quaglia, and P. L. Gilabert, "Reconfigurable DPD based on ANNs for wideband load modulated balanced amplifiers under dynamic operation from 1.8 to 2.4 GHz," *IEEE Trans. Microw. Theory Techn.*, vol. 70, no. 1, pp. 453–465, Jan. 2022.

[14] T. Wang, W. Li, R. Quaglia, and P. L. Gilabert, "Machine-learning assisted optimisation of free-parameters of a dual-input power amplifier for wideband applications," *Sensors*, vol. 21, no. 8, p. 2831, Apr. 2021.

[15] C. Kantana, M. Benosman, R. Ma, and Y. Komatsuzaki, "A system approach for efficiency enhancement and linearization technique of dual-input Doherty power amplifier," *IEEE J. Microw.*, vol. 3, no. 1, pp. 115–133, Jan. 2023.

[16] T. Reveyrand, A. Courty, M. Portelance, P. Medrel, P. Bouysse, and J.-M. Nébus, "Automatic vector signal generator calibration method suitable for multiport large-signal measurements," in *Proc. ARFTG Microw. Meas. Conf.*, 2019, pp. 1–4.

[17] M. Mengozzi et al., "Wideband automated tuning of ka-band dual input Doherty MMIC PA using Bayesian optimization," in *Proc. 18th Eur. Microw. Integr. Circuits Conf. (EuMIC)*, Sep. 2023, pp. 1–4.

[18] C. Schulze et al., "A VNA-based wideband measurement system for large-signal characterization of multiport circuits," *IEEE Trans. Microw. Theory Techn.*, vol. 72, no. 1, pp. 638–647, Jan. 2024.

[19] P. I. Frazier, "A tutorial on Bayesian optimization," 2018, *arXiv:1807.02811*.

[20] P. Chen, B. M. Merrick, and T. J. Brazil, "Bayesian optimization for broadband high-efficiency power amplifier designs," *IEEE Trans. Microw. Theory Techn.*, vol. 63, no. 12, pp. 4263–4272, Dec. 2015.

[21] J. Peng, S. He, B. Wang, Z. Dai, and J. Pang, "Digital predistortion for power amplifier based on sparse Bayesian learning," *IEEE Trans. Circuits Syst. II, Exp. Briefs*, vol. 63, no. 9, pp. 828–832, Sep. 2016.

[22] J. A. Becerra, M. J. Madero-Ayora, R. G. Noguer, and C. Crespo-Cadenas, "On the optimum number of coefficients of sparse digital predistorters: A Bayesian approach," *IEEE Microw. Wireless Compon. Lett.*, vol. 30, no. 12, pp. 1117–1120, Dec. 2020.

[23] M. Sena et al., "Bayesian optimization for nonlinear system identification and pre-distortion in cognitive transmitters," *J. Lightw. Technol.*, vol. 39, no. 15, pp. 5008–5020, Aug. 15, 2021.

[24] J. Cai et al., "Bayesian inference-based behavioral modeling technique for GaN HEMTs," *IEEE Trans. Microw. Theory Techn.*, vol. 67, no. 6, pp. 2291–2301, Jun. 2019.

[25] M. Mengozzi, G. P. Gibiino, A. M. Angelotti, A. Santarelli, C. Florian, and P. Colantonio, "Automatic optimization of input split and bias voltage in digitally controlled dual-input Doherty RF PAs," *Energies*, vol. 15, no. 13, p. 4892, Jul. 2022.

[26] M. Mengozzi et al., "Modulated-input control and linearization of a multi-port millimeter-wave PA by VNA-based calibrated wideband measurements," in *Proc. ARFTG Microw. Meas. Conf.*, 2023, pp. 1–4.

[27] J. Chani-Cahuana, P. N. Landin, C. Fager, and T. Eriksson, "Iterative learning control for RF power amplifier linearization," *IEEE Trans. Microw. Theory Techn.*, vol. 64, no. 9, pp. 2778–2789, Sep. 2016.

[28] C. E. Rasmussen and C. K. I. Williams, *Gaussian Processes for Machine Learning* (Adaptive computation and machine learning). Cambridge, MA, USA: MIT Press, 2006.

[29] M. Malu, G. Dasarathy, and A. Spanias, "Bayesian optimization in high-dimensional spaces: A brief survey," in *Proc. 12th Int. Conf. Inf., Intell., Syst. Appl. (IISA)*, Jul. 2021, pp. 1–8.

[30] M. Mengozzi, A. M. Angelotti, G. P. Gibiino, C. Florian, and A. Santarelli, "Joint dual-input digital predistortion of supply-modulated RF PA by surrogate-based multi-objective optimization," *IEEE Trans. Microw. Theory Techn.*, vol. 70, no. 1, pp. 35–49, Jan. 2022.

[31] M. F. Haider, F. You, S. He, T. Rahkonen, and J. P. Aikio, "Predistortion-based linearization for 5G and beyond millimeter-wave transceiver systems: A comprehensive survey," *IEEE Commun. Surveys Tuts.*, vol. 24, no. 4, pp. 2029–2072, 4th Quart., 2022.

[32] A. M. Angelotti, G. P. Gibiino, C. Florian, and A. Santarelli, "Broadband error vector magnitude characterization of a GaN power amplifier using a vector network analyzer," in *IEEE MTT-S Int. Microw. Symp. Dig.*, Aug. 2020, pp. 747–750.

[33] D. Mikrut et al., "A brief overview of reconfigurable PA technologies," in *Proc. IEEE Wirel. Microw. Tech. Conf.*, Apr. 2024, pp. 1–4.

Mattia Mengozzi (Member, IEEE) received the Ph.D. degree in electronics, telecommunications, and information technology engineering from the University of Bologna, Bologna, Italy, in 2024.

He has been with the Department of Electrical, Electronic, and Information Engineering "Guglielmo Marconi," University of Bologna, since 2020, where he is currently a Post-Doctoral Researcher. His scientific interests involve digital predistortion, microwave measurements, and active load–pull characterization of nonlinear microwave devices.

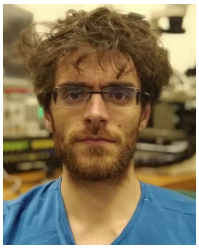

Alberto Maria Angelotti (Member, IEEE) received the Ph.D. degree in electronics, telecommunications, and information technology engineering from the University of Bologna, Bologna, Italy, in 2021.

Since 2017, he has been with the Department of Electrical, Electronic, and Information Engineering "Guglielmo Marconi," University of Bologna, where he is currently a Post-Doctoral Researcher. His research interests include microwave instrumentation, nonlinear measurements, characterization of gallium nitride devices, and power amplifiers.

Gian Piero Gibiino (Member, IEEE) received the dual Ph.D. degree from the University of Bologna, Bologna, Italy, and KU Leuven, Leuven, Belgium, in 2016.

He is currently an Assistant Professor with the Department of Electrical, Electronic, and Information Engineering "Guglielmo Marconi," University of Bologna. His primary research interests include microwave instrumentation and measurement, as well as the experimental evaluation and modeling of microwave devices and circuits.

Dr. Gibiino is an Affiliate Member of the MTT-2 Design Automation and MTT-3 Microwave Measurements Committees.

Christoph Schulze (Graduate Student Member, IEEE) received the B.Eng. degree in communication engineering from the HTW University of Applied Sciences, Berlin, Germany, in 2014, and the M.Sc. degree in electrical engineering from the Technical University of Berlin, Berlin, in 2018.

Since 2020, he has been with the Ferdinand-Braun-Institut gGmbH (FBH), Berlin, where he is currently a Scientific Assistant. His research interests include MMIC power amplifier design and wideband modulated measurements on modified vector network analyzers.

Corrado Florian (Member, IEEE) received the Ph.D. degree in electronic and computer science engineering from the University of Bologna, Bologna, Italy, in 2004.

He is currently an Associate Professor of microwave electronics and power electronics with the Department of Electrical, Electronic and Information Engineering (DEI), University of Bologna. His research interests include microwave monolithic circuit design, hybrid RF circuit design, nonlinear dynamic circuit characterization and modeling, microwave device characterization and modeling, and power electronic circuit design.

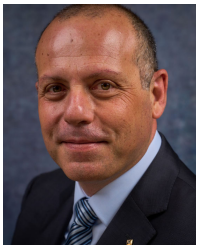

Paolo Colantonio (Fellow, IEEE) received the Laurea degree in electronics engineering and the Ph.D. degree in microelectronics and telecommunications from the University of Rome Tor Vergata, Rome, Italy, in 1994 and 2000, respectively.

He is a Full Professor of microwave electronics at the University of Rome Tor Vergata. His research activities are mainly focused on the field of microwave and millimeter-wave electronic devices, and in particular on the design criteria for nonlinear microwave subsystems and high-efficiency power amplifiers. He is the author or co-author of more than 300 scientific papers. He authored the book *High Efficiency RF and Microwave Solid State Power Amplifiers* (Wiley, 2009), three book chapters, four contributions to the *Encyclopedia on Microwave Electronics* (Wiley), and one international patent.

Dr. Colantonio was elevated as a Fellow for his contribution to microwave power amplifiers in 2024. He has been the Chair of EuMIC 2022 and currently is an Associate Editor of IEEE MICROWAVE AND WIRELESS LETTERS.

Olof Bengtsson (Senior Member, IEEE) received the B.Sc. degree in electrical engineering from the University of Gävle, Gävle, Sweden, in 1997, and the Lic.Tech. and Ph.D. degrees from the Department of Solid State Electronics (SSE), Ångström Laboratory, Uppsala University, Uppsala, Sweden, in 2006 and 2008, respectively.

From 1998 to 2009, he taught microwave engineering at the University of Gävle. Since April 2009, he has been with the Ferdinand-Braun-Institut (FBH), Berlin, Germany, where he is currently the Head of the RF Power Laboratory and the Group Leader of Microwave Measurements. His research interests include large-signal characterization of GaN devices for SISO and MIMO systems and the design of efficient discrete and integrated RF power amplifier systems based on load and supply modulation.

Dr. Bengtsson has been a member of the MTT-12 Microwave High-Power Techniques Committee, since 2018.

Alberto Santarelli (Member, IEEE) received the Laurea degree (cum laude) in electronic engineering and the Ph.D. degree in electronics and computer science from the University of Bologna, Bologna, Italy, in 1991 and 1996, respectively.

He was a Research Assistant with the Research Centre for Computer Science and Communication Systems, Italian National Research Council (IEIIT-CNR), Bologna, from 1996 to 2001. In 2001, he joined the Department of Electrical, Electronic and Information Engineering "Guglielmo Marconi" (DEI), University of Bologna, where he currently is an Associate Professor. During his academic career he has been a Lecturer of high-frequency electronic circuits, applied electronics, and power electronics. His main research interests are related to nonlinear characterization and modeling of electron devices and nonlinear circuit design.

Prof. Santarelli is a member of the European Microwave Association (EuMA).

Open Access funding provided by 'Alma Mater Studiorum - Università di Bologna' within the CRUI CARE Agreement